FERMILAB-PUB-74-118-E #1A
PR.L

SCALING VARIABLE DISTRIBUTIONS IN HIGH ENERGY INELASTIC NEUTRINO INTERACTIONS*

B. Aubert+, A. Benvenuti, D. Cline, W. T. Ford, R. Imlay, T. Y. Ling
A. K. Mann, F. Messing, J. Pilcher‡, D. D. Reeder
C. Rubbia, R. Stefanski, and L. Sulak

Department of Physics
Harvard University
Cambridge, Massachusetts 02138

Department of Physics
University of Pennsylvania
Philadelphia, Pennsylvania 19174

Department of Physics
University of Wisconsin
Madison, Wisconsin 53706

Fermilab
Batavia, Illinois 60510

ABSTRACT

Measured distributions in the scaling variables x and y obtained from the reactions $\nu_\mu(\bar{\nu}_\mu)$ + nucleon → $\mu^-(\mu^+)$ + hadrons at high energy are presented. The x-distributions are consistent with scale invariance. The x- and y-distributions are used to perform the first test of charge symmetry invariance in high energy neutrino interactions.

In a recent paper[1] we reported (i) a measurement of the total cross section for neutrino interactions σ_ν as a function of neutrino energy E_ν up to 150 GeV, and (ii) measurements of the ratio of the antineutrino to the neutrino total cross sections $\sigma_{\bar{\nu}}/\sigma_\nu$ up to 70 GeV. Within experimental error, these results are consistent with V-A coupling, Bjorken scale invariance[2] and the spin $\frac{1}{2}$ parton model[3]. To test these ideas further at high energies, we present here the experimental distributions in the scaling variables $x = q^2/2ME_h$ and $y = E_h/E_\nu$ for neutrinos and antineutrinos, where $q^2 = 4E_\nu E_\mu \sin^2(\theta_\mu/2)$, E_h is the energy of the hadron cascade resulting from the neutrino-nucleon collision, and M is the nucleon mass. As before[1], we identify positive and negative charged final state muons with incident antineutrinos and neutrinos, respectively.

The experimental method was described earlier.[1,4] Briefly, an enriched beam of neutrinos or antineutrinos at Fermilab impinged on a pure liquid scintillator ionization calorimeter (target-detector) in which the neutrino-nucleon interaction occurred, and in which the hadron energy E_h was measured. The vector momentum of the emerging muon p_μ was measured in a magnetic spectrometer directly downstream of the target-detector. The energy of the incident neutrino was then computed from the sum $(E_h + E_\mu)$. Data were obtained with neutrino and antineutrino spectra generated in proton-nucleus collisions with proton energies E_p of 300 and 400 GeV.

Useful interactions took place in a fiducial region of the ionization calorimeter of cross sectional area $(2.4 \times 2.4)m^2$ and length along the beam of 4.1 m. The total area and length of the ionization calorimeter are $(3 \times 3)m^2$ and 7.2 m, respectively. Quasielastic and Δ-production events[1] were eliminated from the scaling variable distributions by means of the combined criteria $W < 1.6$ GeV and $q^2 < 1.0$ GeV^2, where W is the invariant

hadron mass.

The energy response of the ionization calorimeter was calibrated with pions of known energies between 15 and 150 GeV incident on the front of the calorimeter. The measured response of the calorimeter at any energy within that interval is Gaussian with σ = 12%. There is no evidence of a high energy tail at the 1% level at any energy. A low energy calibration point is provided by muons traversing the detector. The response of the muon spectrometer to muons of known momentum is approximately Gaussian with $\sigma \simeq 15\%$ for any muon momentum less than about 80 GeV. These resolution functions, and also that for θ_μ, are included in the calculation of the expected scaling variable distributions described below.

There are shown in Fig. 1 the directly observed distributions (histograms) in x for neutrinos and antineutrinos, combining data taken at 300 and 400 GeV. To exhibit the dependence on $E_\nu(E_{\bar{\nu}})$, the distributions are plotted for two different regions of neutrino and antineutrino energy.[5] For comparison we show also in Fig. 1 the corresponding x-distributions calculated by assuming scale invariance and the simplifying relations among the nucleon structure functions, viz: $2xF_1(x) = F_2(x)$, $xF_3(x) = -F_2(x)$, and $F_i(x) = \bar{F}_i(x)$, where $\bar{F}_i(x)$ refers to antineutrino-nucleon scattering. We have also used the form of $F_2(x)$ obtained from electroproduction experiments[6] (for $x \gtrsim 0.1$), and included incident neutrino and antineutrino spectra[1] and the geometric detection efficiency of the apparatus[1,7] in obtaining the calculated distributions, which are compared with the uncorrected experimental distributions, both normalized to the same area.

The shapes of the observed and calculated x-distributions in Fig. 1 indicate that the x-distributions for neutrinos and antineutrinos are essentially the same, and are not significantly dependent on $E_\nu(E_{\bar{\nu}})$. In Fig. 2

are plotted the measured y-distributions for neutrinos and antineutrinos in the same regions of $E_\nu (E_{\bar\nu})$ as before, with the calculated distributions included for comparison. The observed x- and y-distributions for neutrinos are consistent with the complex of assumptions that enter the calculated distributions, and with earlier data.[8,9]

The y-distributions for antineutrinos, however, are not completely consistent with the simplest form expected from lower energy ($3 < E_{\bar\nu} < 10$ GeV) data[8], viz, $dN/dy \sim (1-y)^2$. For $E_{\bar\nu} < 30$ GeV (Fig. 2b), the experimental y-distribution is not in evident disagreement with that form, but for $E_{\bar\nu} > 30$ GeV (Fig. 2d), the observed y-distribution has 43 events with $y > 0.5$ out of a total of 145, i.e., $(30 \pm 5)\%$, where $(1-y)^2$ multiplied by the detection efficiency predicts less than 10%.

A somewhat more general analysis of the y-distributions may be made by relaxing the assumption that $xF_3(x) = -F_2(x)$. We write the scale invariant differential cross section for inelastic neutrino (antineutrino)-nucleon collisions in the form

$$\frac{d^2\sigma^{\nu,\bar\nu}}{dxdy} = \frac{G^2 ME_\nu}{\pi} F_2(x) \left\{ 1 - y(1 \mp B^{\nu,\bar\nu}) + \frac{y^2}{2}(1 \mp B^{\nu,\bar\nu}) + \frac{y^2}{2} R_L^{\nu,\bar\nu} \right\} \qquad (1)$$

where the upper signs are to be taken for neutrinos, $B^\nu = -xF_3(x)/F_2(x)$, $R_L^\nu = \left[2xF_1(x) - F_2(x) \right] / F_2(x)$ and $B^{\bar\nu} = -x\bar F_3(x)/\bar F_2(x)$, etc. From the positivity conditions, $| xF_3(x) | \leq 2xF_1(x) \leq F_2(x)$, it follows that $R_L \leq 0$, and therefore the term in R_L cannot contribute to the excess of events observed at $y > 0.5$. With $R_L = 0$, eq. (1) is equivalent to a parametrization which mixes a y-independent term and a $(1-y)^2$ term in arbitrary proportions.

Assuming that charge symmetry invariance holds, the ratio of antineutrino to neutrino cross sections integrated over all x and y is $\sigma^{\bar\nu}/\sigma^\nu = (2-\bar B)/(2+\bar B)$,

where $\bar{B}$ is the average value of B(x). One obtains $\bar{B} = 0.9 \pm 0.2$ from the ratio $\sigma^{\bar{\nu}}/\sigma^{\nu} = 0.37 \pm 0.1$ measured[1] at a mean energy of about 40 GeV, and $\bar{B} \approx 0.85$ at lower neutrino energies.[8]

The dependence on x of the y-distributions has been investigated by partitioning the data of Fig. 2 between the regions $x < 0.1$ and $x \geq 0.1$. We have also divided the data by the relative detection efficiency to display the corrected experimental distributions. The results for $0.6 > x \geq 0.1$ for neutrinos and antineutrinos are shown in Figs. 3a and 3b, where it is seen that the excess of events at high-y in the antineutrino distribution has largely disappeared. In Figs. 3c and 3d are shown the corrected y-distributions for neutrinos and antineutrinos in the $x < 0.1$ region. Note the striking difference between the antineutrino y-distributions in the two x-regions.

Apart from resolution effects that influence the lowest bin in y, the experimental distributions in Figs. 3a and 3b are fit to eq. (1) with the values $B^{\nu} = 1.4 \pm 0.6$ and $B^{\bar{\nu}} = 0.6 \pm 0.2$, which are consistent with the value of $\bar{B}$ given above. The y-distributions of Figs. 3c and 3d, however, yield $B^{\nu} = 1.3 \pm 0.6$ and $B^{\bar{\nu}} = -1.2\ ^{+0.8}_{-1.3}$.

If charge symmetry is assumed, B(x) can be determined using eq. (1) for each value of x from the ratios of antineutrino and neutrino cross sections integrated over all y. The x-distributions in Fig. 1 were combined, corrected for detection efficiency and normalized to the value $\sigma^{\bar{\nu}}/\sigma^{\nu} = 0.37$. The results are shown in Fig. 4 where it is seen that B(x) is constant within experimental error over the entire x-range, $x < 0.5$. These results are statistically insensitive to the possible decrease of B(x) at very small x conjectured in the parton model.

To test charge symmetry invariance, we compare the values of B determined separately from x- and y-distributions and total cross section measurements. In Fig. 4 are shown, in addition to the values of B(x) from the x-distributions, the four values of $B^{\nu}(x)$ and $B^{\bar{\nu}}(x)$ obtained from the four y-distributions of Fig. 3. Charge symmetry invariance requires that $B^{\bar{\nu}}(x) = B^{\nu}(x) = B(x)$. In the region $0.6 > x \geq 0.1$, there is agreement within 1 standard deviation among the various measured values of B^{ν}, $B^{\bar{\nu}}$ and B(x), indicating that the data are not inconsistent with charge symmetry. In the region $x < 0.1$, the measured value of $B^{\bar{\nu}}$ differs from the separately determined values of B^{ν} and B(x) by about 3 standard deviations.

We summarize these results as follows. The close similarity of the structure function $F_2(x)$ observed in both electron and neutrino deep inelastic scattering, up to a neutrino energy of about 150 GeV (Fig. 1), and the consistency of the y-distributions in the region $0.6 > x \geq 0.1$ (Figs. 3a and 3b), are further substantive confirmation of scale invariance. In that x-region, the approximate equality of the values of $B^{\nu}(x)$, $B^{\bar{\nu}}(x)$ and B(x) normalized by means of $\sigma^{\bar{\nu}}/\sigma^{\nu}$ constitute evidence for charge symmetry invariance. On the other hand, in the region $x < 0.1$ the excess of events at high-y in the antineutrino y-distribution leads to a value of $B^{\bar{\nu}}$ different from the values of B^{ν} and B(x), which is suggestive of an <u>effective</u> deviation from charge symmetry. This may arise in part from new particle production or from an anomalously large cross section for direct strange particle production.[10] Note that new particle production tends for kinematic reasons to populate preferentially the regions of small x and large y.[11]

It is a pleasure to acknowledge the aid and encouragement of the Fermilab staff. We thank D. Cheng and R. L. Piccioni for their early contributions to this work. We have profited from discussions with Professor S. B. Treiman.

References and Footnotes

* Work supported in part by the U. S. Atomic Energy Commission.

+ On leave of absence from the Laboratoire de l'Accelerateur Lineaire, Orsay, France.

‡ Alfred P. Sloan Foundation Fellow, now at the University of Chicago, Chicago, Ill. 60637.

1. A. Benvenuti et al, Phys. Rev. Letters 32, 125 (1974). See also paper submitted to the XVII International Conference on High Energy Physics, London (1974).

2. J. D. Bjorken, Phys. Rev. 179, 1547 (1969); J. D. Bjorken and E. A. Paschos, Phys. Rev. D1, 3151 (1970).

3. R. P. Feynman, Phys. Rev. Letters 23, 1415 (1969), and in Proc. of the Third Topical Conference on High Energy Collisions, Stony Brook, N. Y., (1969); J. D. Bjorken and E. A. Paschos, Phys. Rev. 185, 1975 (1969).

4. A. Benvenuti et al, Phys. Rev. Letters 30, 1084 (1973).

5. The energy regions into which the data are divided are, to some extent, arbitrary. However, no significant change is made in the results if the data are cut at 25, 40 or 50 GeV. Above 50 GeV, the antineutrino sample becomes statistically limited.

6. G. Miller et al, Phys. Rev. D5, 528 (1972).

7. A. Benvenuti et al, Phys. Rev. Letters 32, 800 (1974); B. Aubert et al, Phys. Rev. Letters 32, 1454 (1974).

8. See, for example, D. H. Perkins, Proc. of the Fifth Hawaii Topical Conference on Particle Physics, ed. P. N. Dobson, Jr , V. Z. Peterson and S. F. Tuan, University of Hawaii, Honolulu (1973); T. Eichten et al, Physics Letters B46, 274 (1973); B46, 281 (1973).

9. B. C. Barish et al, Phys. Rev. Letters 31, 565 (1973).

10. S. L. Glashow, J. Illiopolos and L. Maiani, Phys. Rev. D2, 1285 (1970); A. de Rujula, H. Georgi, S. L. Glashow and H. R. Quinn, Harvard Preprint (1973); G. Altarelli, N. Cabibbo, L. Maiani and R. Petronzio, CERN Preprint TH-1757 (1974).

11. S. L. Adler, NAL preprint 74/39 TH; D. Cline, Proc. of the IV International Conference on Neutrino Physics and Astrophysics, Philadelphia (1974), to be published; M. K. Gaillard, NAL Report FN-259 (1974).

Figure Captions

Fig. 1. Experimental distributions (histograms) in $x = q^2/2ME_h$ and calculated distributions (solid lines) expected from scale invariance using $F_2(x)$ from electroproduction and simplifying relations among the structure functions (see text).

Fig. 2. Experimental and calculated distributions (assuming $B = 1$) in $y = E_h/E_\nu$. The fall-off in the first bin in y in (a) and (b) is due to the joint selection criteria $W > 1.6$ GeV and $q^2 > 1.0$ GeV^2.

Fig. 3. Corrected experimental y-distributions for the region $0.6 > x \geq 0.1$ (a) and (b), and for the region $x < 0.1$ (c) and (d). Points at $y = 0.05$ are omitted because they are sensitive to resolution corrections. Points at $y = 0.95$ in (a) and (b) are omitted because they are sensitive to efficiency corrections. Calculated curves for different values of B^ν and $B^{\bar{\nu}}$ are also shown in (a) and (b).

Fig. 4. Plot of the values of $B(x)$, $B^\nu(x)$ and $B^{\bar{\nu}}(x)$ obtained from the experimental x- and y-distributions in the regions $x < 0.1$ and $0.6 > x \geq 0.1$. The three points in the $x < 0.1$ region, all of which should be plotted at $x = 0.05$, are shifted slightly with respect to each other for improved clarity.

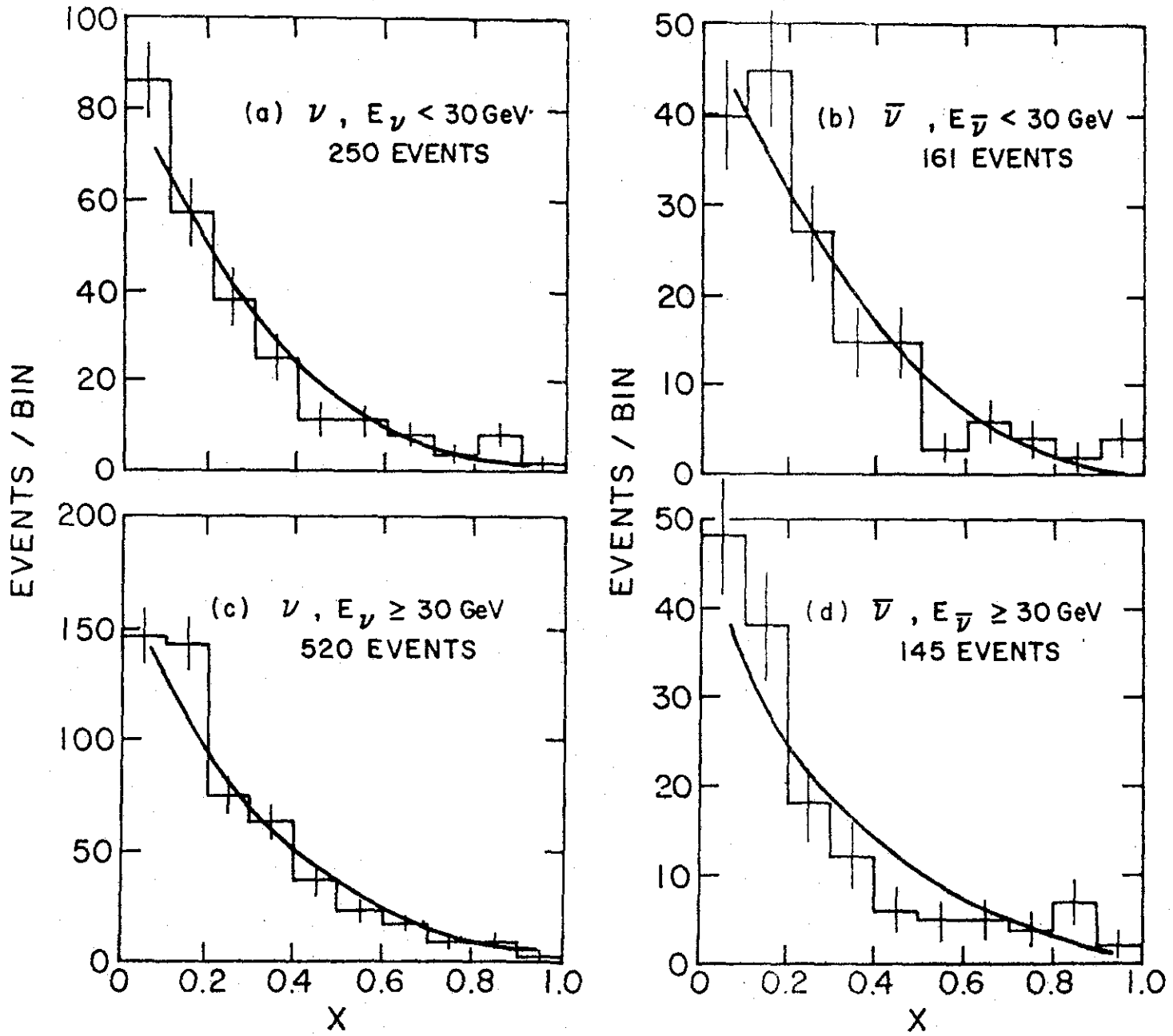
(a) ν , E_ν < 30 GeV
250 EVENTS
(b) ν̄ , E_ν̄ < 30 GeV
161 EVENTS
(c) ν , E_ν ≥ 30 GeV
520 EVENTS
(d) ν̄ , E_ν̄ ≥ 30 GeV
145 EVENTS
EVENTS / BIN
X

Fig. 1

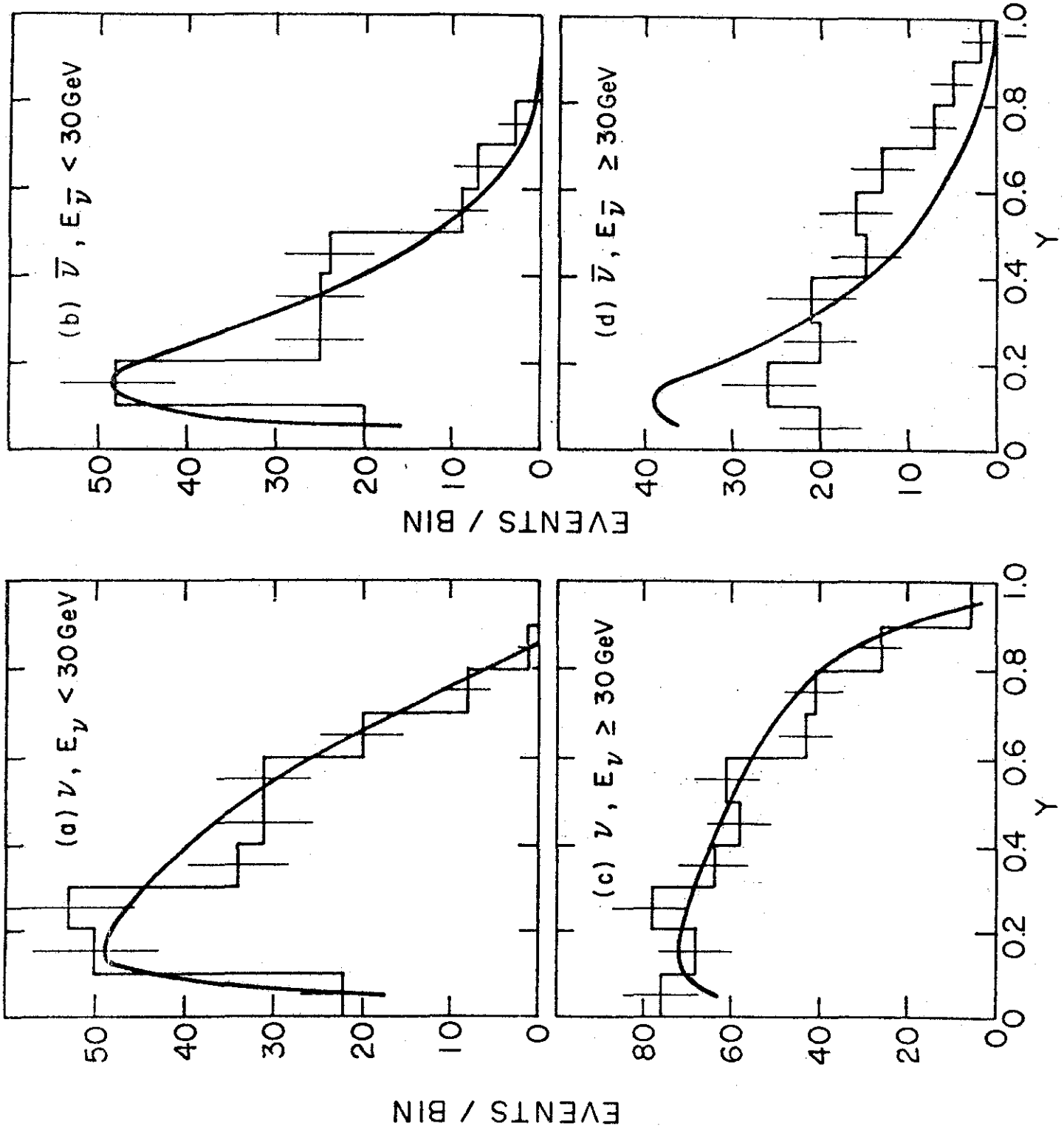

Fig. 2

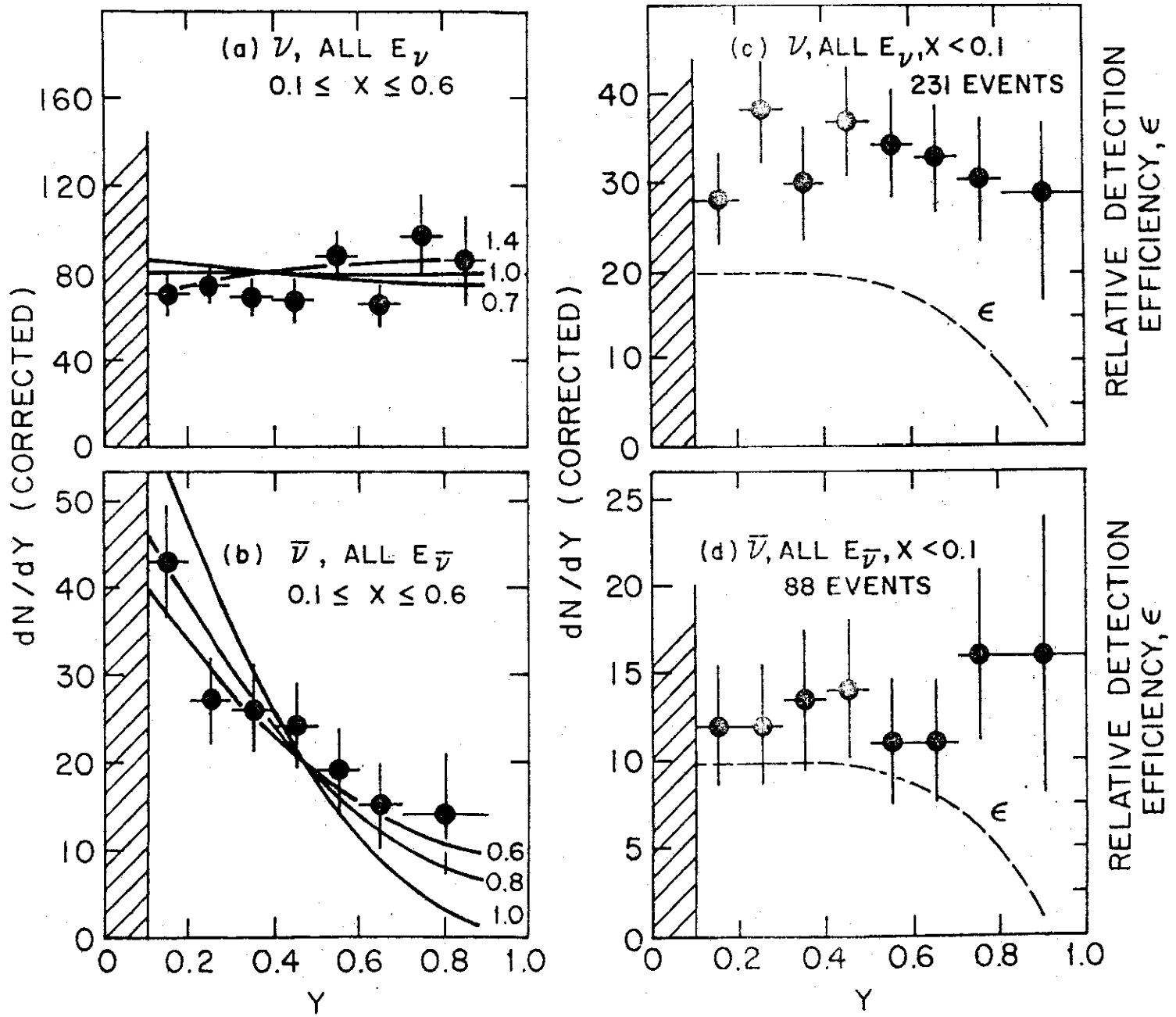
(a) ν, ALL E_ν
0.1 ≤ X ≤ 0.6
1.4
1.0
0.7
(b) ν̄, ALL E_ν̄
0.1 ≤ X ≤ 0.6
0.6
0.8
1.0
dN/dY (CORRECTED)
Y
(c) ν, ALL E_ν, X < 0.1
231 EVENTS
(d) ν̄, ALL E_ν̄, X < 0.1
88 EVENTS
ε
RELATIVE DETECTION EFFICIENCY, ε

Fig. 3

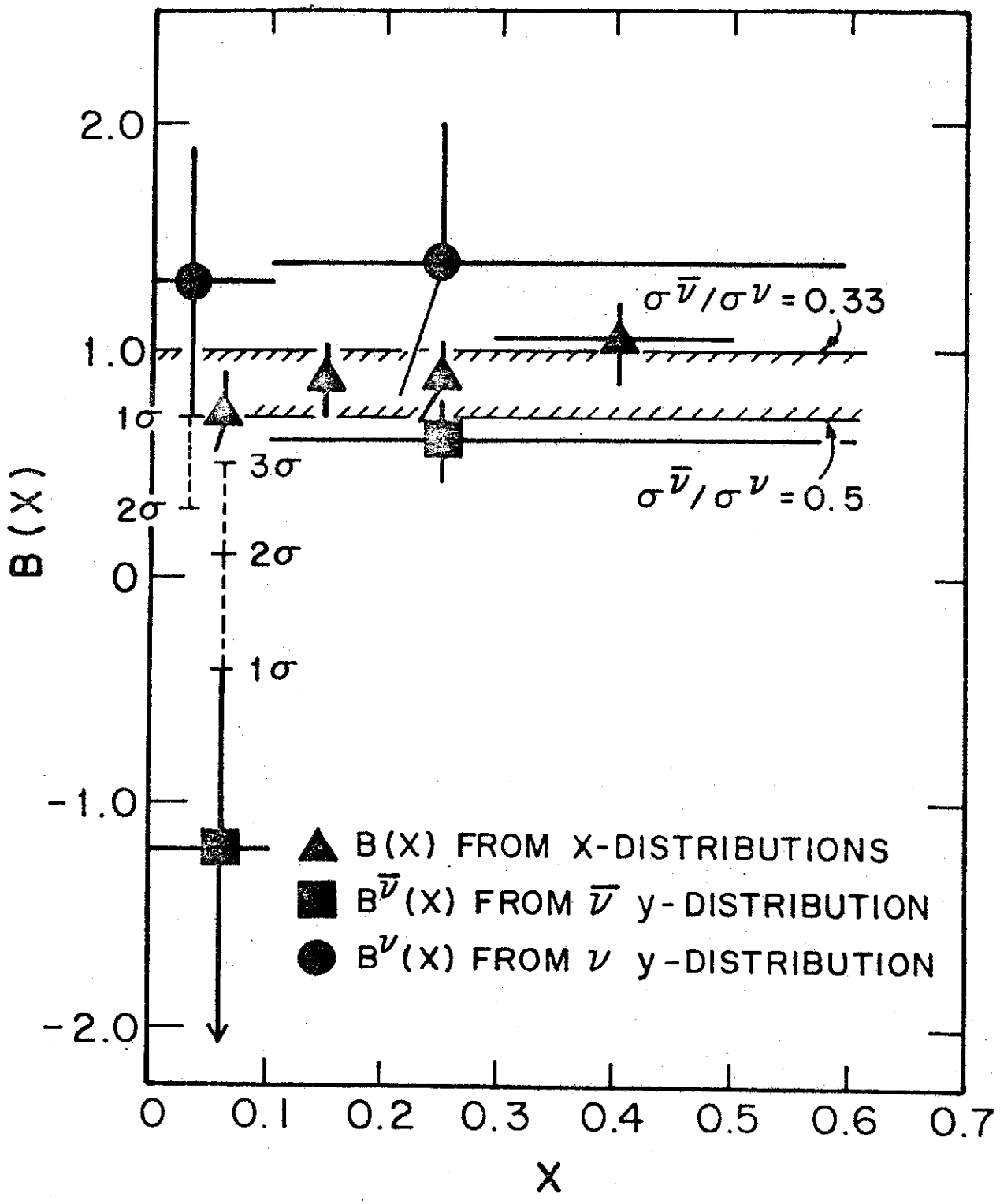
2.0
1.0
1σ
2σ
0
-1.0
-2.0
B(X)
3σ
2σ
1σ
$\sigma^{\bar{\nu}}/\sigma^{\nu} = 0.33$
$\sigma^{\bar{\nu}}/\sigma^{\nu} = 0.5$
B(X) FROM X-DISTRIBUTIONS
$B^{\bar{\nu}}(X)$ FROM $\bar{\nu}$ y-DISTRIBUTION
$B^{\nu}(X)$ FROM ν y-DISTRIBUTION
0
0.1
0.2
0.3
0.4
0.5
0.6
0.7
X

Fig. 4